Theor Chem Acc (2012) 131:1084
DOI 10.1007/s00214-011-1084-8

REGULAR ARTICLE

Electron correlation methods based on the random phase approximation

Henk Eshuis · Jefferson E. Bates · Filipp Furche

Received: 15 June 2011 / Accepted: 16 September 2011

Abstract In the past decade, the random phase approximation (RPA) has emerged as a promising post-Kohn–Sham method to treat electron correlation in molecules, surfaces, and solids. In this review, we explain how RPA arises naturally as a zero-order approximation from the adiabatic connection and the fluctuation-dissipation theorem in a density functional context. This is contrasted to RPA with exchange (RPAX) in a post-Hartree–Fock context. In both methods, RPA and RPAX, the correlation energy may be expressed as a sum over zero-point energies of harmonic oscillators representing collective electronic excitations, consistent with the physical picture originally proposed by Bohm and Pines. The extra factor 1/2 in the RPAX case is rigorously derived. Approaches beyond RPA are briefly summarized. We also review computational strategies implementing RPA. The combination of auxiliary expansions and imaginary frequency integration methods has lead to recent progress in this field, making RPA calculations affordable for systems with over 100 atoms. Finally, we summarize benchmark applications of RPA to various molecular and solid-state properties, including relative energies of conformers, reaction energies involving weak and covalent interactions, diatomic potential energy curves, ionization potentials and electron affinities, surface adsorption energies, bulk cohesive energies and lattice constants. RPA barrier heights for an extended benchmark set are presented. RPA is an order of magnitude more accurate than semi-local functionals such as B3LYP for non-covalent interactions rivaling the best empirically parametrized methods. Larger but systematic errors are observed for processes that do not conserve the number of electron pairs, such as atomization and ionization.

Keywords Electronic structure theory · Density functional theory · Random phase approximation · Resolution-of-the-identity (RI) approximation · Van-der-Waals forces · Thermochemistry

1 Introduction

The random phase approximation (RPA) is one of the oldest non-perturbative methods for computing the ground-state correlation energy of many-electron systems. In 1962, when the first issue of *Theoretica Chimica Acta* was published, RPA had already been in existence for 11 years and was reaching its first bloom in solid-state physics. The term "random phase approximation" was apparently first used in the groundbreaking series of three papers entitled "A Collective Description of Electron Interactions," which appeared between 1951 and 1953 [1–3]. In this work, Bohm and Pines attempted to solve the many-electron problem for the uniform electron gas by a transformation to a much simpler coupled harmonic oscillator problem describing long-range plasma oscillations plus a short-range correction.

Published as part of the special collection of articles celebrating the 50th anniversary of Theoretical Chemistry Accounts/Theoretica Chimica Acta.

Electronic supplementary material The online version of this article (doi:10.1007/s00214-011-1084-8) contains supplementary material, which is available to authorized users.

H. Eshuis · J. E. Bates · F. Furche (✉)
Department of Chemistry, University of California,
1102 Natural Sciences II, Irvine, CA 92697-2025, USA
e-mail: filipp.furche@uci.edu

H. Eshuis
e-mail: henk.eshuis@uci.edu

J. E. Bates
e-mail: batesj@uci.edu

Published online: 14 January 2012

Bohm and Pines showed that this is possible if cross-terms arising from density oscillations with different phases can be neglected, hence the name RPA. Within the RPA of Bohm and Pines, the ground-state correlation energy is given by the zero-point vibrational energy (ZPVE) of the oscillators plus a short-range correction that can be treated perturbatively. This physically appealing picture probably had a strong influence on the development of diagrammatic many-body perturbation theory (MBPT), which treats the ground-state correlation energy in analogy to the vacuum self-energy of quantum electrodynamics. Indeed, in 1957, Gell-Mann and Brueckner obtained the RPA result for the uniform gas correlation energy by summation of all ring diagrams in the MBPT expansion [4], see Fig. 1.

The random phase approximation made its first appearance in chemistry in 1964, when McLachlan and Ball pointed out that time-dependent Hartree–Fock (HF) theory is equivalent to RPA with exchange (RPAX) [5]. In the following decades, RPAX was widely used to compute molecular electronic excitation energies and transition moments and triggered the development of polarization propagator methods in the 1970s [6]. RPAX was rarely applied to molecular correlation energies, partly due to its comparatively high computational cost and partly because applications to small systems showed little promise [7]. Perhaps the most serious limitation of RPAX is its sensitivity to instabilities of the HF reference state. This and the emergence of coupled cluster theory effectively halted further development of RPAX-based correlation methods in the late 1970s. Attempts to make RPAX more stable by iteration of excitation operators ("higher-order RPA") [8, 9] were later shown to be related to the antisymmetrized geminal power method [10].

On the side of density functional theory, Langreth and Perdew [11, 12] and Gunnarsson and Lundqvist [13] established the adiabatic connection (AC) formalism in the mid 1970s. The AC underlies most modern post-Kohn–Sham (KS) correlation treatments that attempt to compute the ground-state correlation energy using the KS determinant as a reference. A crucial difference between the AC formalism and post-HF methods that the ground-state density is *independent* of the coupling strength in the former but not in the latter. Langreth and Perdew showed that RPA arises as a natural zero-order approximation if the AC

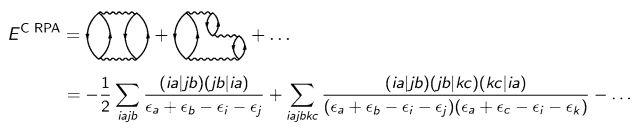

$$= -\frac{1}{2}\sum_{iajb}\frac{(ia|jb)(jb|ia)}{\epsilon_a+\epsilon_b-\epsilon_i-\epsilon_j} + \sum_{iajbkc}\frac{(ia|jb)(jb|kc)(kc|ia)}{(\epsilon_a+\epsilon_b-\epsilon_i-\epsilon_j)(\epsilon_a+\epsilon_c-\epsilon_i-\epsilon_k)} - \cdots$$

Fig. 1 MBPT expansion of the RPA correlation energy using Goldstone diagrams. $(ia|jb)$ denotes an electron repulsion integral in Mulliken notation, and ϵ_p is a canonical Kohn–Sham orbital eigenvalue. Indices $i, j, \ldots$ denote occupied, $a, b, \ldots$ virtual, and $p, q, \ldots$ general orbitals

framework is combined with the fluctuation-dissipation theorem [14]. RPA was the basis for the development of the first van der-Waals density functionals of Langreth–Lundqvist type in the 1990s [15]. Dobson pioneered the use of RPA for the seamless treatment of long-range dispersion interactions [16, 17]. Only in 2001, RPA using a KS reference was first applied to molecules [18].

In the past decade, RPA has seen a remarkable revival. This review aims to introduce RPA in its modern form to a wider audience and explain why RPA-based electron correlation methods seem more attractive than ever. The present work reflects our personal views on the subject, and we do not claim to be exhaustive in view of a rapidly growing literature on RPA. In Sect. 2, we outline the derivation of RPA starting from the AC formalism. We also include a section on RPAX using a HF reference, highlighting the common aspects and differences between the two approaches (see also the recent review by Heßelmann and Görling [134]). An important feature of RPA is that it can be systematically improved; some beyond-RPA approaches are briefly addressed in Sect. 2.3. Section 3 contains an overview of recent RPA implementations. Recent progress in this area has helped transform RPA from a theory of mostly formal interest to a viable computational tool. In Sect. 4, we summarize recent results on the performance of RPA for a variety of molecular properties. Section 5 concludes our review.

2 Theory

2.1 Kohn–Sham reference

2.1.1 Adiabatic connection

The starting point for post-KS density functional theory is the adiabatic connection Hamiltonian [11, 13]

$$\hat{H}^\alpha = \hat{T} + \hat{V}^\alpha[\rho] + \alpha\hat{V}_{ee}. \tag{1}$$

$\hat{T}$ denotes the kinetic energy operator of the electrons. The dimensionless coupling strength parameter α scales the electron–electron interaction $\hat{V}_{ee}$. The local multiplicative one-particle potential $\hat{V}^\alpha[\rho]$ constrains [19] the one-particle density ρ^α of the ground state $|\Psi_0^\alpha\rangle$ to equal the interacting ground-state density ρ for all α,

$$\rho^\alpha(x) = \rho^\alpha(x)\big|_{\alpha=1} = \rho(x). \tag{2}$$

$x = (\mathbf{r}, \sigma)$ denotes space–spin coordinates. Thus, for $\alpha = 1$, the physical system of N interacting electrons is recovered, while $\alpha = 0$ corresponds to the KS system whose ground state is the KS determinant $|\Phi_0\rangle = |\Psi_0^\alpha\rangle\big|_{\alpha=0}$.

The interacting ground-state energy functional may be expressed as the energy expectation value of the Kohn–Sham determinant plus a correction for correlation,

$$E_0[\rho] = \langle \Phi_0[\rho]|\hat{H}|\Phi_0[\rho]\rangle + E_C[\rho], \tag{3}$$

where $\hat{H} = \hat{H}^{\alpha}\big|_{\alpha=1}$ is the physical Hamiltonian. While the explicit form of $E_C[\rho]$ as a functional of the density is unknown, it can be expressed by a coupling strength integral [11, 13],

$$E_C[\rho] = \int_0^1 d\alpha W_C^{\alpha}[\rho]. \tag{4}$$

The coupling strength integrand is the difference potential energy of the electron interaction

$$W_C^{\alpha}[\rho] = \langle \Psi_0^{\alpha}[\rho]|\hat{V}_{ee}|\Psi_0^{\alpha}[\rho]\rangle - \langle \Phi_0[\rho]|\hat{V}_{ee}|\Phi_0[\rho]\rangle. \tag{5}$$

2.1.2 Density fluctuations

An important hierarchy of approximations to $W_C^{\alpha}[\rho]$ is based on the idea to reexpress the potential energy of the electron–electron interaction in terms of density fluctuations. To this end, it is convenient to express $\hat{V}_{ee}$ in second quantized form,

$$\hat{V}_{ee} = \frac{1}{2}\sum_{pqrs}\langle pq|rs\rangle \hat{c}_p^{\dagger}\hat{c}_q^{\dagger}\hat{c}_s\hat{c}_r, \tag{6}$$

where $\hat{c}_p^{\dagger}$ and their adjoints denote electron creation and annihilation operators, and $\langle pq|rs\rangle$ is a two-electron repulsion integral in Dirac notation. To take advantage of the locality of the electron–electron interaction, we introduce electron field operators,

$$\hat{\psi}^{\dagger}(x) = \sum_p \phi_p^*(x)\hat{c}_p^{\dagger}; \tag{7}$$

$\phi_p(x)$ denotes a Kohn–Sham spin orbital. Defining the two-particle density operator,

$$\hat{P}(x_1, x_2) = \frac{1}{2}\hat{\psi}^{\dagger}(x_1)\hat{\psi}^{\dagger}(x_2)\hat{\psi}(x_2)\hat{\psi}(x_1), \tag{8}$$

the electron interaction operator may be written as

$$\hat{V}_{ee} = \int dx_1 dx_2 \frac{\hat{P}(x_1, x_2)}{|\mathbf{r}_1 - \mathbf{r}_2|}. \tag{9}$$

Our goal is to factorize $\hat{P}(x_1, x_2)$ into products of one-particle operators. Using the fermion anticommutation relations, we obtain

$$\hat{P}(x_1, x_2) = \frac{1}{2}(\hat{\rho}(x_1)\hat{\rho}(x_2) - \delta(x_1 - x_2)\hat{\rho}(x_1)), \tag{10}$$

where $\hat{\rho}$ is the one-particle density operator

$$\hat{\rho}(x) = \hat{\psi}^{\dagger}(x)\hat{\psi}(x). \tag{11}$$

This may be further rewritten using the density fluctuation operator $\Delta\hat{\rho}(x) = \hat{\rho}(x) - \rho(x)$,

$$\hat{P}(x_1, x_2) = \frac{1}{2}(\Delta\hat{\rho}(x_1)\Delta\hat{\rho}(x_2) + \hat{\rho}(x_1)\rho(x_2) + \rho(x_1)\hat{\rho}(x_2) - \rho(x_1)\rho(x_2).-\delta(x_1 - x_2)\hat{\rho}(x_1)). \tag{12}$$

The last identity and Eq. 9 may be combined to evaluate the coupling strength integrand, Eq. 5. Because the density is independent of α, all one-electron terms cancel, yielding the simple result

$$W_C^{\alpha} = \frac{1}{2}\int dx_1 dx_2 \times \frac{\langle \Psi_0^{\alpha}|\Delta\hat{\rho}(x_1)\Delta\hat{\rho}(x_2)|\Psi_0^{\alpha}\rangle - \langle \Phi_0|\Delta\hat{\rho}(x_1)\Delta\hat{\rho}(x_2)|\Phi_0\rangle}{|\mathbf{r}_1 - \mathbf{r}_2|}. \tag{13}$$

2.1.3 Fluctuation-dissipation theorem

Equation 13 expresses the coupling strength integrand W_C^{α} as an expectation value of *products* of the density fluctuation operator $\Delta\hat{\rho}$. Using the completeness of the electronic states $|\Psi_n^{\alpha}\rangle$ at any α,

$$\sum_n |\Psi_n^{\alpha}\rangle\langle\Psi_n{}^{\alpha}| = \mathbf{1}, \tag{14}$$

the expectation value of $\Delta\hat{\rho}(x_1)\Delta\hat{\rho}(x_2)$, a *two-particle* operator, may be factorized into products of *one-particle* transition densities,

$$\langle \Psi_0^{\alpha}|\Delta\hat{\rho}(x_1)\Delta\hat{\rho}(x_2)|\Psi_0^{\alpha}\rangle = \sum_{n\neq 0}\rho_{0n}^{\alpha}(x_1)\rho_{0n}^{\alpha}(x_2). \tag{15}$$

Here, we used that the ground-state expectation value of $\Delta\hat{\rho}$ is zero, and

$$\rho_{0n}^{\alpha}(x) = \langle \Psi_0^{\alpha}|\hat{\rho}(x)|\Psi_n^{\alpha}\rangle = \langle \Psi_0^{\alpha}|\Delta\hat{\rho}(x)|\Psi_n^{\alpha}\rangle. \tag{16}$$

Combining Eqs. 4, 13, and 15, we obtain an exact expression for the ground-state correlation energy,

$$E_C = \int_0^1 d\alpha \sum_{n\neq 0}\Big(E_H[\rho_{0n}^{\alpha}] - E_H[\rho_{0n}^{(0)}]\Big). \tag{17}$$

$E_H[\rho]$ denotes the Hartree or classical Coulomb energy functional,

$$E_H[\rho] = \frac{1}{2}\int dx_1 dx_2 \frac{\rho(x_1)\rho(x_2)}{|\mathbf{r}_1 - \mathbf{r}_2|}. \tag{18}$$

This result is remarkable, because it expresses the correlation energy entirely in terms of one-particle quantities, the transition densities. Transition densities are accessible from response theory. This becomes obvious if the zero-temperature fluctuation-dissipation theorem [14] is used to express the sum in Eq. 15 by a frequency integral of the density–density response function at coupling strength α,

$$\langle \Psi_0^\alpha | \Delta\hat{\rho}(x_1)\Delta\hat{\rho}(x_2) | \Psi_0^\alpha \rangle = -\int_0^\infty \frac{d\omega}{\pi} \mathrm{Im}\chi^\alpha(\omega, x_1, x_2). \quad (19)$$

The latter follows, e.g., from the Lehmann representation [20] of χ^α,

$$\chi^\alpha(\omega, x_1, x_2) = -\sum_{n\neq 0}\left(\frac{\rho_{0n}^\alpha(x_1)\rho_{0n}^\alpha(x_2)}{\Omega_{0n}^\alpha - \omega - i\eta} + \frac{\rho_{0n}^\alpha(x_1)\rho_{0n}^\alpha(x_2)}{\Omega_{0n}^\alpha + \omega + i\eta}\right), \quad (20)$$

where Ω_{0n}^α denote excitation energies, and $i\eta$ is a small contour distortion making χ^α analytical in the upper complex plane. By Eqs. 19, 15, and 4, the ground-state correlation energy may be entirely expressed in terms of χ^α [11, 12],

$$E_\mathrm{C}[\rho] = -\frac{1}{2}\int_0^1 d\alpha \int_0^\infty \frac{d\omega}{\pi}\mathrm{Im} \times \int dx_1 dx_2 \frac{\chi^\alpha(\omega, x_1, x_2) - \chi^{(0)}(\omega, x_1, x_2)}{|\mathbf{r}_1 - \mathbf{r}_2|}. \quad (21)$$

2.1.4 Connection to time-dependent density functional theory

The density–density response function χ^α or, alternatively, the transition densities ρ_{0n}^α, are accessible from time-dependent density functional theory (TDDFT) [21]. χ^α satisfies the Dyson-type equation [22]

$$\chi^\alpha = \chi^{(0)} + \chi^{(0)} f_\mathrm{HXC}^\alpha \chi^\alpha. \quad (22)$$

The frequency-dependent Hartree, exchange, and correlation kernel can be decomposed into the bare Coulomb interaction and an exchange and correlation (XC) piece,

$$f_\mathrm{HXC}^\alpha(\omega, x_1, x_2) = \alpha\frac{1}{|\mathbf{r}_1 - \mathbf{r}_2|} + f_\mathrm{XC}^\alpha(\omega, x_1, x_2). \quad (23)$$

Alternatively, the transition densities can be computed from the response of the time-dependent KS density matrix, leading to the symplectic eigenvalue problem [23, 24]

$$(\Lambda^\alpha - \Omega_{0n}^\alpha \Delta)|X_{0n}^\alpha, Y_{0n}^\alpha\rangle = 0. \quad (24)$$

The super-vectors X_{0n}^α and Y_{0n}^α are defined on the product space $L_\mathrm{occ} \times L_\mathrm{virt}$ and $L_\mathrm{occ} \times L_\mathrm{virt}$, respectively, where L_occ and L_virt denote the one-particle Hilbert spaces spanned by occupied and virtual static KS molecular orbitals (MOs). We use indices $i, j, \ldots$ for occupied, $a, b, \ldots$ for virtual, and $p, q, \ldots$ for general MOs and assume that all MOs are real. The super-operator

$$\Lambda^\alpha = \begin{pmatrix} \mathbf{A}^\alpha & \mathbf{B}^\alpha \\ \mathbf{B}^\alpha & \mathbf{A}^\alpha \end{pmatrix} \quad (25)$$

contains the so-called orbital rotation Hessians,

$$(A+B)_{iajb}^\alpha = (\epsilon_a - \epsilon_i)\delta_{ij}\delta_{ab} + 2\alpha\langle ij|ab\rangle + 2f_{\mathrm{XC}iajb}^\alpha, \quad (26)$$

$$(A-B)_{iajb}^\alpha = (\epsilon_a - \epsilon_i)\delta_{ij}\delta_{ab}. \quad (27)$$

ϵ_i and ϵ_a denote the energy eigenvalues of canonical occupied and virtual KS MOs. The eigenvectors $|X_{0n}^\alpha, Y_{0n}^\alpha\rangle$ satisfy the symplectic normalization constraint

$$\langle X_{0n}^\alpha, Y_{0n}^\alpha | \Delta | X_{0n}^\alpha, Y_{0n}^\alpha \rangle = 1, \quad (28)$$

where

$$\Delta = \begin{pmatrix} \mathbf{1} & \mathbf{0} \\ \mathbf{0} & -\mathbf{1} \end{pmatrix}. \quad (29)$$

The real-space transition density can be extracted from the eigenvectors $|X_{0n}^\alpha, Y_{0n}^\alpha\rangle$ according to

$$\rho_{0n}^\alpha(x) = \sum_{ia}(X+Y)_{ia}^\alpha \phi_i(x)\phi_a(x). \quad (30)$$

Using Eq. 17, the correlation energy in terms of X_{0n}^α and Y_{0n}^α is thus [18]

$$E_\mathrm{C} = \frac{1}{2}\int_0^1 d\alpha \sum_{iajb}\langle ij|ab\rangle\left(\sum_{n\neq 0}(X+Y)_{0nia}^\alpha (X+Y)_{0njb}^\alpha - \delta_{ij}\delta_{ab}\right). \quad (31)$$

2.1.5 Random phase approximation

The XC kernel as a functional of the ground-state density is not explicitly known. Within RPA, the XC kernel is set to zero,

$$f_\mathrm{XC}^{\alpha\mathrm{RPA}}(\omega, x_1, x_2) = 0. \quad (32)$$

Thus, RPA within a density functional context is identical to the time-dependent Hartree approximation.

Within RPA, the correlation energy takes a particularly simple form. Applying the Hellmann–Feynman theorem to the eigenvalue problem (Eq. 24) within RPA, it follows that

$$\frac{d\Omega_{0n}^{\alpha\mathrm{RPA}}}{d\alpha} = \sum_{iajb}(X+Y)_{ia}^{\alpha\mathrm{RPA}}\langle ij|ab\rangle(X+Y)_{jb}^{\alpha\mathrm{RPA}} = 2E_\mathrm{H}[\rho_{0n}^{\alpha\mathrm{RPA}}]. \quad (33)$$

Thus, the RPA correlation energy may be written as

$$E_\mathrm{C}^\mathrm{RPA} = \frac{1}{2}\int_0^1 d\alpha \sum_n\left(\frac{d\Omega_{0n}^{\alpha\mathrm{RPA}}}{d\alpha} - \left.\frac{d\Omega_{0n}^{\alpha\mathrm{RPA}}}{d\alpha}\right|_{\alpha=0}\right). \quad (34)$$

The coupling strength integration can thus be carried out analytically, yielding

$$E_{\mathrm{C}}^{\mathrm{RPA}} = \frac{1}{2}\sum_n \left(\Omega_{0n}^{\mathrm{RPA}} - \Omega_{0n}^{\mathrm{D}}\right). \tag{35}$$

$\Omega_{0n}^{\mathrm{RPA}}$ is an RPA excitation energy at full coupling, and Ω_{0n}^{D} is an RPA excitation energy to first order in α. Using the unitary invariance of the trace in Eq. 35, the sum over the Ω_{0n}^{D} may be replaced by the sum over the RPA excitation energies within the Tamm–Dancoff approximation (TDA) [25],

$$E_{\mathrm{C}}^{\mathrm{RPA}} = \frac{1}{2}\sum_n \left(\Omega_{0n}^{\mathrm{RPA}} - \Omega_{0n}^{\mathrm{TDARPA}}\right). \tag{36}$$

Equation 36 expresses the RPA correlation energy as a ZPVE difference of harmonic oscillators, where each oscillator corresponds to an electronic excitation, in agreement with Bohm's and Pines's original idea.

2.1.6 Connection to Green's function methods

RPA may be derived from the GW approximation to the one-electron self energy [26, 27]. This self-energy is the derivative of the functional

$$\Phi^{\mathrm{GW}} = \frac{1}{2}\mathrm{tr}\{\ln(1 + iVG_{\mathrm{S}}G_{\mathrm{S}})\}, \tag{37}$$

with respect to the non-interacting Green's function G_{S} [28]. V denotes the bare Coulomb interaction. $-i\Phi^{\mathrm{GW}}$ plays the role of the exchange-correlation energy in the Klein functional of the total energy. The GW method is widely used to compute band structures of solids [29, 30] because it incorporates basic screening physics beyond the single-particle picture.

2.2 Hartree–Fock reference

2.2.1 Correlation energy from coupling strength integration

Post-HF methods are usually based on the Møller–Plesset partitioning of the Hamiltonian [31],

$$\hat{H}_{\mathrm{HF}}^{\alpha} = \hat{H}_{\mathrm{HF}}^{(0)} + \alpha\hat{H}_{\mathrm{HF}}^{(1)}. \tag{38}$$

The zero-order Hamiltonian is the Fock operator,

$$\hat{H}_{\mathrm{HF}}^{(0)} = \hat{T} + \hat{V}_{ne} + \hat{J} + \hat{K}, \tag{39}$$

where $\hat{V}_{ne}$ denotes the operator of the nucleus–electron attraction; $\hat{J}$ and $\hat{K}$ are the Coulomb and non-local exchange operators, respectively.

$$\hat{H}_{\mathrm{HF}}^{(1)} = \hat{H} - \hat{H}_{\mathrm{HF}}^{(0)} = \hat{V}_{ee} - \hat{J} - \hat{K} \tag{40}$$

is the so-called fluctuation potential. At zero coupling strength, the ground state $|\Psi_{\mathrm{HF0}}^{\alpha}\rangle$ equals the HF determinant $|\Phi_{\mathrm{HF0}}\rangle$. Except for the physical system at $\alpha = 1$, $\hat{H}_{\mathrm{HF}}^{\alpha}$ and the ground state $|\Psi_{\mathrm{HF0}}^{\alpha}\rangle$ are different from the adiabatic connection Hamiltonian $\hat{H}^{\alpha}$ and its ground state $|\Psi_0^{\alpha}\rangle$ defined by Eq. 1: $|\Psi_0^{\alpha}\rangle$ is constrained to yield the interacting ground-state density for any α, while the density of $|\Phi_{\mathrm{HF0}}\rangle$ changes with α; on the other hand, $|\Phi_{\mathrm{HF0}}\rangle$ minimizes the energy expectation value

$$\langle\Phi_{\mathrm{HF0}}|\hat{H}|\Phi_{\mathrm{HF0}}\rangle = E_{\mathrm{HF}} = E_{\mathrm{HF}}^{(0)} + E_{\mathrm{HF}}^{(1)}, \tag{41}$$

while the KS determinant $|\Phi_0\rangle$ does not.

For a HF reference, the interacting ground-state energy E_0 equals the HF energy plus the HF correlation energy,

$$E_0 = E_{\mathrm{HF}} + E_{\mathrm{HFC}}. \tag{42}$$

The latter thus differs from the KS correlation energy defined in Eq. 3. The HF correlation energy may be expressed as an integral over coupling strength,

$$E_{\mathrm{HFC}} = \int_0^1 d\alpha \frac{dE_{\mathrm{HF0}}^{\alpha}}{d\alpha} - E_{\mathrm{HF}}^{(1)} = \int_0^1 d\alpha W_{\mathrm{HFC}}^{\alpha} \tag{43}$$

By virtue of the Hellmann–Feynman theorem, the coupling strength integrand is given by an expectation value difference of the fluctuation potential,

$$W_{\mathrm{HFC}}^{\alpha} = \langle\Psi_{\mathrm{HF0}}^{\alpha}|\hat{H}_{\mathrm{HF}}^{(1)}|\Psi_{\mathrm{HF0}}^{\alpha}\rangle - \langle\Phi_{\mathrm{HF0}}|\hat{H}_{\mathrm{HF}}^{(1)}|\Phi_{\mathrm{HF0}}\rangle. \tag{44}$$

This may be contrasted with the adiabatic connection integrand, Eq. 5, which does not contain any one-particle terms.

2.2.2 Factorization of the fluctuation potential

To apply factorization techniques along the lines of Sect. 2.1.2, we rewrite the fluctuation potential operator as

$$\hat{H}_{\mathrm{HF}}^{(1)} = \sum_{pqrs} \langle pq|rs\rangle \hat{U}_{pqrs}, \tag{45}$$

where

$$\hat{U}_{pqrs} = \frac{1}{2}\hat{c}_p^{\dagger}\hat{c}_q^{\dagger}\hat{c}_s\hat{c}_r - \hat{\gamma}_{pr}\gamma_{\mathrm{HF}qs} + \hat{\gamma}_{ps}\gamma_{\mathrm{HF}qr}. \tag{46}$$

$\hat{\gamma}_{pq} = \hat{c}_p^{\dagger}\hat{c}_q$ is the density matrix operator in second quantization, and

$$\gamma_{\mathrm{HF}pq} = \langle\Phi_{\mathrm{HF0}}|\hat{\gamma}_{pq}|\Phi_{\mathrm{HF0}}\rangle \tag{47}$$

is the density matrix of the HF ground-state determinant. Since the ground-state density matrix

$$\gamma_{pq}^{\alpha} = \langle\Psi_{\mathrm{HF0}}^{\alpha}|\hat{\gamma}_{pq}|\Psi_{\mathrm{HF0}}^{\alpha}\rangle \tag{48}$$

(and the density) varies with α, fluctuation operators do not lead to simplifications here. However, using the Fermion anticommutation relations, $\hat{U}$ can still be factorized into one-particle operators,

$$\hat{U}_{pqrs} = \frac{1}{2}\hat{\gamma}_{pr}\hat{\gamma}_{qs} - \hat{\gamma}_{pr}\gamma_{\mathrm{HF}qs} + \hat{\gamma}_{ps}\left(\gamma_{\mathrm{HF}qr} - \frac{1}{2}\delta_{qr}\right). \tag{49}$$

While $\hat{U}_{pqrs}$ as a whole is antisymmetric under the exchange of p and q or r and s, the individual terms in the last equation are not. To preserve the antisymmetry of $\hat{U}$ and thus of the two-particle density matrix when approximations are introduced, it is convenient to use the explicitly antisymmetrized expression

$$\begin{aligned}\hat{U}_{pqrs} = {} & \frac{1}{4}(\hat{\gamma}_{pr}\hat{\gamma}_{qs} - \hat{\gamma}_{ps}\hat{\gamma}_{qr}) - \hat{\gamma}_{pr}\left(\gamma_{\mathrm{HF}qs} - \frac{1}{4}\delta_{qs}\right) \\ & + \hat{\gamma}_{ps}\left(\gamma_{\mathrm{HF}qr} - \frac{1}{4}\delta_{qr}\right).\end{aligned} \tag{50}$$

2.2.3 Fluctuation-dissipation theorem

In analogy to Sect. 2.1.3, we use the completeness of the states $|\Psi^{\alpha}_{\mathrm{HF}n}\rangle$ to factorize expectation values of products of two density matrix operators,

$$\langle\Psi^{\alpha}_{\mathrm{HF}0}|\hat{\gamma}_{pr}\hat{\gamma}_{qs}|\Psi^{\alpha}_{\mathrm{HF}0}\rangle = \sum_{n\neq 0}\gamma^{\alpha}_{0npq}\gamma^{\alpha\dagger}_{0nqs} + \gamma^{\alpha}_{pq}\gamma^{\alpha}_{qs}. \tag{51}$$

Instead of transition densities $\rho^{\alpha}_{0n}(x)$, we now encounter the more general one-particle transition density matrices at coupling strength α,

$$\gamma^{\alpha}_{0npq} = \langle\Psi^{\alpha}_{\mathrm{HF}0}|\hat{\gamma}_{pq}|\Psi^{\alpha}_{\mathrm{HF}n}\rangle. \tag{52}$$

The additional ground-state term arises because fluctuation operators are not used here, as explained previously.

Defining the Hartree plus exchange functional of the one-particle density matrix

$$E^{(1)}[\gamma] = \frac{1}{2}\sum_{pqrs}\langle pq|rs\rangle(\gamma_{pr}\gamma^{\dagger}_{qs} - \gamma_{ps}\gamma^{\dagger}_{qr}), \tag{53}$$

we obtain the following exact expression for the HF correlation energy:

$$E_{\mathrm{HFC}} = \frac{1}{2}\int_0^1 d\alpha\sum_{n\neq 0}(E^{(1)}[\gamma^{\alpha}_{0n}] - E^{(1)}[\gamma^{(0)}_{0n}]) + \Delta E_{\mathrm{HFC}} \tag{54}$$

It is instructive to compare this result to its density functional equivalent, Eq. 17. The additional factor of 1/2 in Eq. 54 arises from enforcing the antisymmetry of U_{pqrs} in Eq. 50. The correction term ΔE_{HFC}, which is not present in the density functional case, is due to the change of the ground-state density matrix with α,

$$\begin{aligned}\Delta E_{\mathrm{HFC}} = {} & \int_0^1 d\alpha\sum_{pqrs}\langle pq|rs\rangle\Big\{\frac{1}{4}\left(\gamma^{\alpha}_{pr}\gamma^{\alpha}_{qs} - \gamma^{\alpha}_{ps}\gamma^{\alpha}_{qr} - \gamma_{\mathrm{HF}pr}\gamma_{\mathrm{HF}qs}\right. \\ & \left. + \gamma_{\mathrm{HF}ps}\gamma_{\mathrm{HF}qr}\right) - \left(\gamma^{\alpha}_{pr} - \gamma_{\mathrm{HF}pr}\right)\left(\gamma_{\mathrm{HF}qs} + \frac{1}{4}\delta_{qs}\right) \\ & + \left(\gamma^{\alpha}_{ps} - \gamma_{\mathrm{HF}ps}\right)\left(\gamma_{\mathrm{HF}qr} + \frac{1}{4}\delta_{qr}\right)\Big\}.\end{aligned} \tag{55}$$

Using the zero-temperature fluctuation-dissipation theorem, the sum over transition density matrices may be expressed by a frequency integral over the density matrix—density matrix response function at coupling strength α,

$$\sum_{n\neq 0}\gamma^{\alpha}_{0npr}\gamma^{\alpha\dagger}_{0nqs} = -\int_0^{\infty}\frac{d\omega}{\pi}\mathrm{Im}\Pi^{\alpha}_{prqs}(\omega). \tag{56}$$

This follows, e.g., from the Lehmann representation of Π^{α} [20],

$$\Pi^{\alpha}_{prqs}(\omega) = -\sum_{n\neq 0}\left(\frac{\gamma^{\alpha}_{0npr}\gamma^{\alpha\dagger}_{0nqs}}{\Omega^{\alpha}_{0n} - \omega - i\eta} + \frac{\gamma^{\alpha\dagger}_{0npr}\gamma^{\alpha}_{0nqs}}{\Omega^{\alpha}_{0n} + \omega + i\eta}\right). \tag{57}$$

The ground-state density matrix γ^{α}_{pr} occurring in $\Delta E_{\mathrm{c\,HF}}$ is accessible from Π^{α} via a partial trace of the two-particle density matrix. Thus, knowledge of Π^{α} is sufficient to compute the HF correlation energy.

2.2.4 Connection to polarization propagator theory

The density matrix–density matrix response function $\Pi^{\alpha}(\omega)$ is identical to the causal polarization propagator. $\Pi^{\alpha}(\omega)$ satisfies the Bethe–Salpeter equation [20]

$$\Pi^{\alpha}(\omega) = \Pi^{(0)}(\omega) + \Pi^{(0)}(\omega)K^{\alpha}(\omega)\Pi^{\alpha}(\omega). \tag{58}$$

The frequency-dependent kernel $K^{\alpha}(\omega)$ may be computed perturbatively. The lowest non-vanishing order in α is

$$K^{(1)}_{prqs}(\omega) = \langle pr|qs\rangle - \langle ps|qr\rangle. \tag{59}$$

2.2.5 Random phase approximation with exchange

The random phase approximation with exchange consists in replacing the kernel $K^{\alpha}(\omega)$ in Eq. 58 with its first-order approximation $\alpha\, K^{(1)}$, which is frequency independent. In addition, the ground-state density matrices γ^{α}_{pq} are replaced by $\gamma_{\mathrm{HF}pq}$, making ΔE_{HFC} vanish. Thus, the RPAX coupling strength integrand is correct to first order in α, and the RPAX correlation energy is correct to $O(\alpha^2)$, that is, it reduces to second-order Møller–Plesset perturbation theory

(MP2) for small α. Within RPAX, the transition density matrices may be written as

$$\gamma_{0npr}^{\mathrm{RPAX}\alpha} = X_{npr}^{\mathrm{RPAX}\alpha} n_p(1-n_r) + Y_{nrp}^{\mathrm{RPAX}\alpha} n_r(1-n_p), \tag{60}$$

where n_p and n_r denote orbital occupation numbers. The super-vectors $|X_n^{\mathrm{RPAX}\alpha}, Y_n^{\mathrm{RPAX}\alpha}\rangle$ satisfy a symplectic eigenvalue problem of the same form as Eq. 24. The RPAX orbital rotation Hessians are [32]

$$(A+B)_{iajb}^{\mathrm{RPAX}\alpha} = (\epsilon_a - \epsilon_i)\delta_{ij}\delta_{ab} + \alpha[2\langle ij|ab\rangle - \langle ij|ba\rangle - \langle ia|jb\rangle], \tag{61}$$

$$(A-B)_{iajb}^{\mathrm{RPAX}\alpha} = (\epsilon_a - \epsilon_i)\delta_{ij}\delta_{ab} + \alpha[\langle ij|ba\rangle - \langle ia|jb\rangle]. \tag{62}$$

Using the Hellmann–Feynman theorem once more, one finds that the excitation energies $\Omega_{0n}^{\mathrm{RPAX}\alpha}$ satisfy

$$\frac{d\Omega_{0n}^{\mathrm{RPAX}\alpha}}{d\alpha} = \frac{1}{2}\sum_{iajb}\Big\{(X+Y)_{ia}^{\mathrm{RPAX}\alpha}[2(ij|ab) - (ij|ba) - (ia|jb)](X+Y)_{jb}^{\mathrm{RPAX}\alpha} + (X-Y)_{ia}^{\mathrm{RPAX}\alpha}[(ij|ba) - (ia|jb)](X-Y)_{jb}^{\mathrm{RPAX}\alpha}\Big\} = 2E^{(1)}[\gamma_{0n}^{\mathrm{RPAX}\alpha}] \tag{63}$$

Again, the coupling strength integration may be carried out analytically, yielding

$$E_{\mathrm{C}}^{\mathrm{RPAX}} = \frac{1}{4}\sum_n\left(\Omega_{0n}^{\mathrm{RPAX}} - \Omega_{0n}^{\mathrm{TDARPAX}}\right). \tag{64}$$

Compared to Eq. 36, Eq. 64 contains an extra factor 1/2 resulting from the antisymmetrization applied in Eq. 50. If the antisymmetrization is not applied, and the exchange part of $K^{(1)}$ is neglected, Eq. 36 is recovered, now using a HF reference. Other combinations such as the RPAx method of Toulouse and coworkers [33, 135] generally do not lead to an analytically integrable coupling strength integral, because the Hellmann–Feynman theorem cannot be used. This also applies to "hybrid" schemes that incorporate only a fraction of exchange [34].

A drawback of RPAX is that it includes spin-flip excitations. For example, for a spin-restricted closed-shell HF ground state, Eq. 64 becomes

$$E_{\mathrm{C}}^{\mathrm{RPAX}}(\mathrm{RHF}) = \frac{1}{4}\sum_n\left(\Omega_{0n\mathrm{S}}^{\mathrm{RPAX}} - \Omega_{0n\mathrm{S}}^{\mathrm{TDARPAX}}\right) + \frac{3}{4}\sum_n\left(\Omega_{0n\mathrm{T}}^{\mathrm{RPAX}} - \Omega_{0n\mathrm{T}}^{\mathrm{TDARPAX}}\right), \tag{65}$$

where subscripts S and T denote singlet and triplet excitation energies, respectively. RPAX spin-flip excitation energies are very sensitive to the quality of the HF reference. Triplet instabilities are common, leading to a breakdown of RPAX and imaginary correlation energies [35]. In contrast, spin-flip excitations cancel out of Eq. 36, because they are the same with and without TDA.

RPAX contains all third-order particle-hole diagrams, albeit with incorrect pre-factors [6, 7, 36, 37]. Direct RPA, Eq. 36, contains ring diagrams only, but the pre-factors are correct.

2.2.6 Connection to coupled cluster theory

From a coupled cluster perspective, RPA is a simplified coupled cluster doubles (CCD) method [38, 39]. The RPAX correlation energy may be written as

$$E_{\mathrm{C}}^{\mathrm{RPAX}} = \frac{1}{4}\mathrm{tr}(\mathbf{B}^{\mathrm{RPAX}}\mathbf{T}), \tag{66}$$

where $B_{iajb}^{\mathrm{RPAX}} = \langle ij|ab\rangle - \langle ij|ba\rangle$. The doubles amplitudes $\mathbf{T}$ are related to the vectors $|X_n^{\mathrm{RPAX}}, Y_n^{\mathrm{RPAX}}\rangle$ at full coupling according to [40]

$$\mathbf{T} = \mathbf{Y}^{\mathrm{RPAX}}\mathbf{X}^{\mathrm{RPAX}-1} \tag{67}$$

and satisfy the ring-CCD equation [9, 41]

$$\mathbf{B}^{\mathrm{RPAX}} + \mathbf{A}^{\mathrm{RPAX}}\mathbf{T} + \mathbf{T}\mathbf{A}^{\mathrm{RPAX}} + \mathbf{T}\mathbf{B}^{\mathrm{RPAX}}\mathbf{T} = \mathbf{0}. \tag{68}$$

Similar relations hold in the KS case for direct RPA [136].

2.3 Beyond RPA

Beyond-RPA methods aim to approximate the beyond-RPA correlation energy

$$E_{\mathrm{C}}^{\mathrm{bRPA}}[\rho] = E_{\mathrm{C}}[\rho] - E_{\mathrm{C}}^{\mathrm{RPA}}[\rho]. \tag{69}$$

Due to the deficiencies of RPAX, most work so far uses direct RPA and a KS reference. Beyond-RPA methods are a rapidly growing field, and we give a brief overview of some important directions only.

2.3.1 Density functional corrections

In the uniform electron gas, corrections to RPA arise from short-range electron interactions. If the same holds for molecules and solids, a generalized gradient approximation (GGA) to $E_{\mathrm{C}}^{\mathrm{bRPA}}[\rho]$ should be accurate, since GGAs are generally believed to work best for short-range interactions [42]. The so-called RPA+ [43] thus approximates beyond-RPA correlation by the beyond-RPA piece of the PBE GGA,

$$E_{\mathrm{C}}^{\mathrm{bRPA}}(\mathrm{RPA+})[\rho] = E_{\mathrm{C}}^{\mathrm{PBE}}[\rho] - E_{\mathrm{C}}^{\mathrm{PBE\,RPA}}[\rho]. \tag{70}$$

While RPA+ improves total molecular correlation energies considerably, energy differences such as atomization energies are essentially unchanged compared to RPA [18]. Recently, Ruzsinszky et al. explained this puzzling result by non-local multi-center correlation that is present in

molecules but not in the uniform electron gas [44]. This hypothesis is corroborated by a considerable improvement upon RPA atomization energies obtained from a non-local correction to RPA [45].

Range-separation methods go one step further, removing all short-range correlation from RPA using a screened interaction [33, 46, 137, 47, 138]. Range separation improves the basis set convergence of RPA correlation energies by largely eliminating the electron coalescence cusp in the pair density. The results of range-separated RPA depend on the adjustable range-separation parameter.

2.3.2 Perturbative corrections

The lowest order non-vanishing correction to RPA is second-order exchange,

$$E_{\mathrm{C}}^{\mathrm{bRPA}}(\mathrm{X2}) = \frac{1}{2}\sum_{iajb}\frac{\langle ij|ab\rangle\langle ij|ba\rangle}{\epsilon_a+\epsilon_b-\epsilon_i-\epsilon_j}. \tag{71}$$

However, $E_{\mathrm{C}}^{\mathrm{bRPA}}(\mathrm{X2})$ does not improve upon RPA systematically because it suffers from the shortcomings of second-order Görling–Levy perturbation theory [48]. The latter is very sensitive to the KS HOMO-LUMO gap and breaks down already for moderately small-gap cases [49].

Based on early work by Freeman [38], Kresse et al. proposed a second-order screened exchange (SOSEX) correction to RPA [50],

$$E_{\mathrm{C}}^{\mathrm{bRPA}}(\mathrm{SOSEX}) = -\frac{1}{2}\sum_{iajb}\langle ij|ba\rangle T_{iajb}, \tag{72}$$

where $\mathbf{T}$ is computed by solving the ring-CCD equation (without exchange). SOSEX is free of one-electron self-correlation, yields much improved total correlation energies, and appears to improve upon RPA atomization energies [50–52]. SOSEX is more stable than bare second-order exchange and finite for small-gap systems and metals. The trade-off for eliminating self-interaction error is the reintroduction of an incorrect dissociation behavior for covalent bonds in a spin-restricted closed-shell treatment [53], see Sect. 4.2.

Recently, Ren and coworkers showed that a perturbative single-excitation correction, which arises in second-order Görling–Levy perturbation theory, leads to an improvement of RPA for weakly interacting systems [54]. Lotrich and Bartlett also obtained improved results for such systems using a correction based on external coupled cluster perturbation theory [139].

2.3.3 Local field corrections

Local field corrections to RPA were first explored for the uniform electron gas by Singwi, Tosi, Land, and Sjölander (STLS) [55], who introduced an XC kernel depending on the pair distribution function to correct RPA at short range. In a broader sense, local field corrections use non-zero XC kernels to improve upon RPA.

A straightforward choice motivated by TDDFT is to use XC kernels derived from semi-local functionals within the adiabatic approximation [56], which replaces f_{XC}^{α} by its static limit,

$$f_{\mathrm{XC}}^{\alpha}(0,x_1,x_2) = \frac{\delta^2 E_{\mathrm{XC}}[\rho]}{\delta\rho(x_1)\delta\rho(x_2)}. \tag{73}$$

However, the spacial locality of these kernels leads to an unphysical divergence in the RPA pair density [34, 57]. Even for the uniform electron gas correlation energy, the adiabatic local-spin density approximation (ALDA) kernel yields poor results [58].

Dobson et al. [59] extended the original STLS model to inhomogeneous systems. The resulting ISTLS method is equivalent to a non-local tensor exchange-correlation kernel in the context of time-dependent current density functional theory [60]. ISTLS yields highly accurate jellium surface energies [61] but apparently has not been applied to molecular systems so far.

2.3.4 Optimized effective potential methods

Kotani and Akai [62] were the first to combine the exact Kohn–Sham exchange potential and RPA correlation [RPA(EXX)]. The Kohn–Sham exchange potential is obtained from the exact exchange using the framework of the optimized effective potential (OEP) method. The exact exchange potential is both non-local and frequency-dependent and is, therefore, expected to show no divergence of the pair density at short interelectronic distances. Hellgren and von Barth [63] applied RPA(EXX) to atoms, reporting good agreement with accurate configuration interaction results.

A disadvantage of OEP methods is the need to compute the inverse of the Kohn–Sham response matrix, which leads to numerical instabilities in conjunction with finite basis set methods [64, 65]. Heßelmann, Ipatov, and Görling developed an approximate scheme that avoids inverses of the Kohn–Sham response matrix [66]. Heßelmann and Görling reported RPA(EXX) correlation energies for small organic molecules that improve considerably upon RPAX correlation energies [67]. Reaction energies involving these molecules are less affected.

3 Implementation

3.1 Diagonalization

In quantum chemistry, the molecular orbitals are usually approximated by a finite linear combination of atom-

centered basis functions (LCAO-MO approach). The expansion coefficients are determined variationally. The finite number of basis functions used results in a finite number of virtual orbitals, which in turn leads to a finite dimension of the RPA eigenvalue problem, Eq. 36. Thus, in a finite basis, the total number of excitation energies is given by $L_{\rm occ} \times L_{\rm virt}$.

The RPA eigenvalue problem may be transformed to a Hermitian eigenvalue problem [18]

$$\mathbf{MZ} = \mathbf{Z\Omega}^2, \qquad \mathbf{ZZ}^{\rm T} = \mathbf{1}, \tag{74}$$

where

$$\mathbf{M} = (\mathbf{A}-\mathbf{B})^{1/2}(\mathbf{A}+\mathbf{B})(\mathbf{A}-\mathbf{B})^{1/2}, \tag{75}$$

is easily computed since $(\mathbf{A}-\mathbf{B})^{1/2}$ is diagonal within RPA, see Eq. 27. Thus, Eq. 36 may be rewritten in terms of the square root of $\mathbf{M}$,

$$E^{\rm C\,RPA} = \frac{1}{2}{\rm tr}(\mathbf{M}^{1/2} - \mathbf{A}). \tag{76}$$

Straightforward evaluation of all excitation energies in Eq. 36 leads to a $\mathcal{O}(N^6)$ scaling with system size N. This follows from the dimension of the eigenvalue problem ($L_{\rm occ} \times L_{\rm virt}$) and from the $\mathcal{O}(N^3)$ scaling of the diagonalization procedure.

The first RPA correlation energies on molecules were obtained by full diagonalization of Eq. 75 [18, 34] combined with a grid-based coupling constant integration. The steep increase in computational cost with system size limited these applications to small molecules (approximately 10 atoms).

3.2 Resolution-of-the-identity approximation

A more efficient method can be obtained by taking advantage of the rank deficiency of the two-electron Coulomb integrals present in Eq. 36. The key idea is to represent the rank deficient orbital product densities in a small number of auxiliary basis functions. Several such methods exist [39, 68–70], but the resolution-of-the-identity (RI) approximation [71] with the Coulomb metric [72] represents an optimum choice for RPA, as explained later. The RI approximation is used extensively and successfully in the context of ground-state density functional theory (DFT) [73] and TDDFT excitation energy calculations [74–76] as well as MP2 [77, 78]. In the RI approximation, the two-electron integrals can be factorized, using Mulliken notation, as

$$(ia|jb)_{\rm RI} = \sum_{PQ}(ia|P)(P|Q)^{-1}(Q|jb) = \sum_{P} S_{iaP}S_{jbP}, \tag{77}$$

where $S_{iaP} = \sum_R (ia|R)L^{-1}_{RP}$, P, Q, R denote atom-centered Gaussian auxiliary basis functions, and L_{RP} is determined by Cholesky decomposition of the two-electron integrals $(P|Q)$

$$(P|Q) = \sum_R L_{PR}L_{QR}. \tag{78}$$

Since the number of auxiliary basis functions $N_{\rm aux}$ increases only linearly with N, it is much more efficient to work with matrix $\mathbf{S}$ instead of the full two-electron matrix $(ia|jb)$. $E^{\rm C\ RIRPA}$ is evaluated by replacing the two-electron integrals in Eq. 76 with $(ia|jb)_{\rm RI}$. Importantly, the error due to RI is quadratic in each RPA excitation energy [79]. Therefore, high accuracy can be achieved with moderately sized auxiliary basis sets. The variational stability of the excitation energies carries over to the RPA correlation energy. Thus, the RIRPA correlation energy is a variational upper bound to the exact RPA correlation energy [79]. This variational property also allows for systematic optimization of the auxiliary basis sets.

Four-index quantities are entirely avoided by evaluating $\mathbf{M}^{1/2}$ as an integral over imaginary frequency [80]

$${\rm tr}\left(\mathbf{M}^{1/2}\right) = 2\int_{-\infty}^{\infty}\frac{d\omega}{2\pi}{\rm tr}\left(\mathbf{1} - \omega^2\left(\mathbf{M}+\omega^2\mathbf{1}\right)^{-1}\right). \tag{79}$$

Within RI, $\mathbf{M} = \mathbf{D}^2 + 2\,\mathbf{D}^{1/2}\,\mathbf{S}\,\mathbf{S}^{\rm T}\,\mathbf{D}^{1/2}$, where $D_{iajb} = D_{ia}\,\delta_{ij}\delta_{ab}$, and $D_{ia} = \epsilon_a - \epsilon_i$, is the diagonal matrix of bare orbital energy differences. The inverse of $\mathbf{M} + \omega^2\,\mathbf{1}$ may be written as

$$\begin{aligned}\left(\mathbf{M}+\omega^2\mathbf{1}\right)^{-1} = {}& \mathbf{D}^{-1}\mathbf{G}(\omega) - 2\mathbf{D}^{-1/2}\mathbf{G}(\omega) \\ & \mathbf{S}(\mathbf{1}_{\rm aux} + \mathbf{Q}(\omega))^{-1}\mathbf{S}^{\rm T}\mathbf{G}(\omega)\mathbf{D}^{-1/2},\end{aligned} \tag{80}$$

where

$$\mathbf{G}(\omega) = \mathbf{D}(\mathbf{D}^2 + \omega^2\mathbf{1})^{-1} \tag{81}$$

is diagonal in the canonical Kohn–Sham orbital basis, and

$$\mathbf{Q}(\omega) = 2\mathbf{S}^{\rm T}\mathbf{G}(\omega)\mathbf{S} \tag{82}$$

is $N_{\rm aux} \times N_{\rm aux}$. Using an analogous expression for tr($\mathbf{A}$), the RPA correlation energy is expressed as

$$E^{\rm C\,RIRPA} = \int_{-\infty}^{\infty}\frac{d\omega}{2\pi}F^{\rm C}(\omega), \tag{83}$$

where the integrand contains $N_{\rm aux} \times N_{\rm aux}$ quantities only,

$$F^{\rm C}(\omega) = \frac{1}{2}{\rm tr}(\ln(\mathbf{1}_{\rm aux} + \mathbf{Q}(\omega)) - \mathbf{Q}(\omega)). \tag{84}$$

Taylor expansion of $\ln(\mathbf{1}_{\rm aux} + \mathbf{Q})$ in Eq. 83 leads to the diagrammatic RPA, where $\mathbf{Q}$ is the equivalent of a single

ring diagram [4], see Fig. 1. The variational upper bound property of RIRPA is maintained in Eq. 83.

The efficient evaluation of Eq. 83 hinges on an efficient quadrature scheme to compute the frequency integral. Eshuis, Yarkony, and Furche used an exponentially converging Clenshaw–Curtis quadrature [81] with a single scaling parameter, which is determined from the orbital energies and the diagonal elements of **M**. RIRPA scales as $\mathcal{O}(N^4 \log N)$. It is straightforward to achieve an additional speed-up by parallelization over the frequency integration grid.

The RI approximation leads to sub-millihartree errors when MP2-optimized auxiliary basis sets are used [83], as shown in Fig. 2 for the HEAT test set [84]. The RI errors are much smaller than the intrinsic errors of RPA. The dependence of the RIRPA correlation energy for the HEAT test set on the number of grid points is shown in Fig. 3. Submillihartree accuracy is achieved for the numerical integration with typically 40–50 grid points using a basis of quadruple-zeta quality. Larger grids are required when core electrons are included. Exceptions arise when contributions from different eigenvalues to the integrand have very different scaling, for example, in small-gap systems. A measure for the spread of the excitation energies is the condition number $\kappa = \Omega_{\max}/\Omega_{\min}$. A large number of grid points are required for large κ.

To address this difficulty, a hybrid scheme was developed, which computes a few small eigenvalues explicitly and the remainder on the grid. Starting from the exact spectral representation of $F^{\mathrm{C}}(\Omega)$ for the n_{lowest} eigenvalues

$$\tilde{F}^{\mathrm{C}} = \frac{1}{2}\sum_{ia}^{n_{\mathrm{lowest}}}\left[\ln\left(1+\frac{\Omega_{ia}^2 - D_{ia}^2}{\omega^2 + D_{ia}^2}\right) - \frac{M_{iaia} - D_{ia}^2}{\omega^2 + D_{ia}^2}\right], \tag{85}$$

we can compute

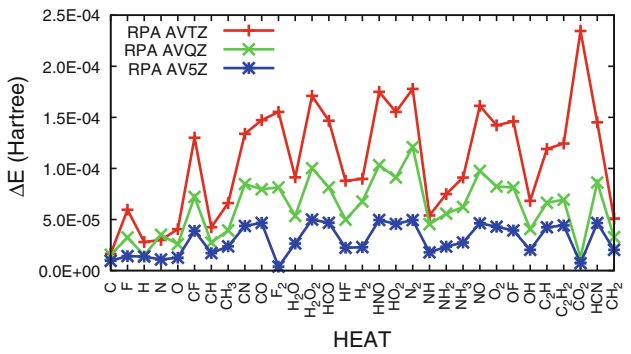

Fig. 2 RI errors ($\Delta E = E^{\mathrm{C\,RIRPA}} - E^{\mathrm{C\,RPA}}$) in all electron RPA correlation energies for the HEAT test set using three of Dunning's correlation consistent basis sets (AVTZ = aug-cc-pVTZ, etc. [82]). (Reprinted with permission from Ref. [79]. Copyright 2010 American Institute of Physics)

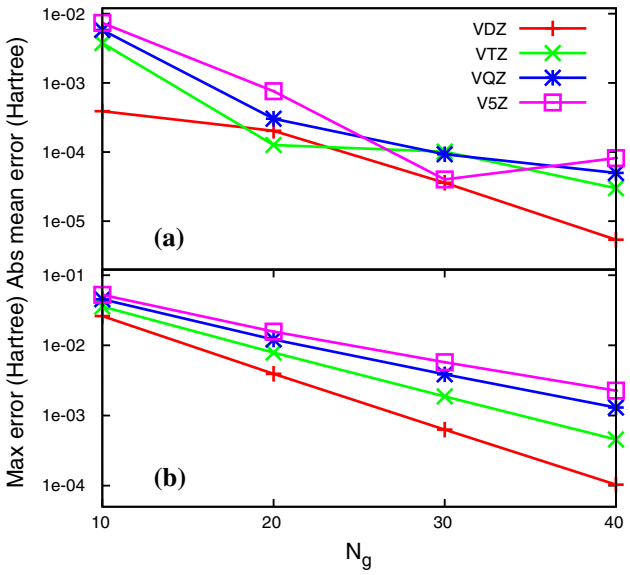

Fig. 3 Absolute mean errors (*a*) and maximum errors (*b*) due to numerical integration for RI-RPA HEAT atomization energies with varying number of grid points N_g and increasing basis set size (V*XZ* = cc-pV*XZ*). (Reprinted with permission from Ref. [79]. Copyright 2010 American Institute of Physics)

$$\begin{aligned}\tilde{E}^{\mathrm{C\,RIRPA}} &= \frac{1}{2}\int_{-\infty}^{\infty}\frac{d\omega}{2\pi}\tilde{F}^{\mathrm{C}}(\omega)\\ &= \frac{1}{2}\sum_{ia}^{n_{\mathrm{lowest}}}\left(\Omega_{ia} - (D_{ia} + (ia|ia)_{\mathrm{RI}})\right)\end{aligned} \tag{86}$$

efficiently if $n_{\mathrm{lowest}} \ll L_{\mathrm{occ}} \times L_{\mathrm{virt}}$. The hybrid RIRPA correlation energy is now given by

$$\begin{aligned}E^{\mathrm{C\,RIRPA}} &= \frac{1}{2}\int_{-\infty}^{\infty}\frac{d\omega}{2\pi}\left(F^{\mathrm{C}}(\omega) - \tilde{F}^{\mathrm{C}}(\omega)\right)\\ &\quad + \frac{1}{2}\sum_{ia}^{n_{\mathrm{lowest}}}\left(\Omega_{ia} - (D_{ia} + (ia|ia)_{\mathrm{RI}})\right).\end{aligned} \tag{87}$$

The new integrand, $F^{\mathrm{C}} - \tilde{F}^{\mathrm{C}}$, is associated with a smaller condition number $\tilde{\kappa} = \Omega_{\max}/\Omega_{n_{\mathrm{lowest}}+1}$. Preliminary results show microhartree accuracy can be reached if eigenvalues less than approximately 0.05 Hartree are treated explicitly.

The RIRPA scheme leads to considerable speed-ups, as demonstrated for a set of polyacenes in Fig. 4. Also, the memory requirements are much smaller, because 4-index objects are avoided altogether. For the Grubbs II Ru catalyst, which consists of 117 atoms, using def2-TZVP basis sets [85] on C,H, and N and def2-QZVPP [85] on the other atoms, see Sect. 4.1, the RIRPA correlation energy can be computed in approximately 8 CPU hours on 16 processors of a single 2.2 GHz AMD Opteron 6174 node using multithreaded BLAS routines and 10 Gb of memory [86]. The number of excitations involved is 287036, which is clearly out of reach for full diagonalization.

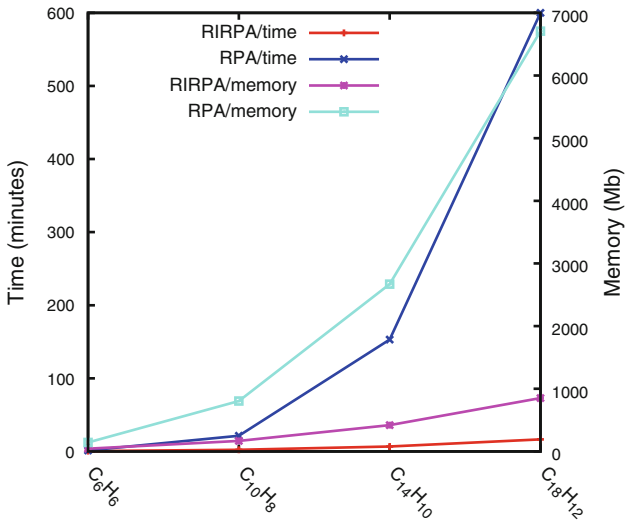

Fig. 4 RIRPA timings and memory usage for polyacenes of increasing size compared to RPA results obtained through direct diagonalization. Def2-TZVPP basis sets were used, and the calculations were performed on a single CPU of a Xeon X5560 2.80 GHz workstation

3.3 Other implementations

3.3.1 Ring coupled cluster doubles

Random phase approximation correlation energies can also be computed from the ring approximation to coupled cluster doubles theory (rCCD) [39] by solving for the amplitudes in Eq. 68. This can be easily done starting from an existing CCD code and removing all but ring contractions. rCCD correlation energies can, therefore, be obtained from minor modifications. However, the computational cost scales as $\mathcal{O}(N^6)$ and I/O as $\mathcal{O}(N^5)$ because of the need to store all doubles amplitudes on disk.

Scuseria et al. proposed the use of Cholesky decompositions to reduce the scaling by writing

$$(ia|jb) = \sum_A u_{ia}^A u_{jb}^A, \tag{88}$$

and

$$-T_{ij}^{ab} = \sum_A \theta_{ia}^A \theta_{jb}^A. \tag{89}$$

This is possible in direct RPA, because both $(ia|jb)$ and $-T_{ij}^{ab}$ are positive definite. The rCCD expression can then be rewritten as

$$-T_{ij}^{ab} = -\frac{1}{\epsilon_i + \epsilon_j - \epsilon_a - \epsilon_b}\left(\sum_A u_{ia}^A u_{jb}^A - \sum_{AB} u_{ia}^A N^{AB} \theta_{jb}^B - \sum_{AB} \theta_{ia}^A M^{AB} \theta_{jb}^B - \sum_{ABC} \theta_{ia}^A N^{AB} M^{BC} \theta_{jb}^C\right), \tag{90}$$

where $M^{AB} = \sum_{kc} \theta_{kc}^A u_{kc}^B$ and $N^{AB} = \sum_{kc} u_{kc}^A \theta_{kc}^B$. Iterative methods can be used to solve Eq. 90 for the amplitudes, although no implementations seem to be available so far.

3.3.2 Plane wave implementations

In plane wave implementations of RPA, the use of auxiliary basis expansions is fairly straightforward. Core electrons must be treated by pseudopotentials or projector augmented wave methods [87]. The starting point for plane wave codes [87–90] is the expression by Langreth and Perdew [12]

$$E^{\mathrm{cRPA}} = \frac{1}{2}\int_{-\infty}^{\infty} \frac{d\omega}{2\pi} \mathrm{tr}(\ln(\mathbf{1} + \chi(i\omega)W) - \chi(i\omega)W), \tag{91}$$

where χ is the Kohn–Sham density–density response function, and W is the bare Coulomb interaction. The number of virtual orbitals depends on the size of the plane wave basis, which is determined by an energy cutoff E_{cut}. In addition, the correlation energy depends on the length of the maximum reciprocal lattice vector G_{cut}^{χ} and its energy E_{cut}^{χ}. These quantities determine the size of the plane wave expansion of the response function. Convergence with respect to E_{cut}^{χ} is slow, but good results can be obtained by using an extrapolation scheme [87]. The frequency integration in Eq. 91 is done using Gauss–Legendre quadrature. Alternatively, the rCCD expression can be used as a starting point [50].

4 Applications

4.1 Non-covalent interactions

Non-covalent interactions play an important role in chemistry, physics, and biology, e.g., in DNA, enzymes, and graphene sheets [91–93]. A striking example are the relative energies of alkane conformers, which crucially depend on mid-range non-covalent electronic interactions between two bonds separated by another bond (1–3 interactions) [94–97]. These systems exemplify the failure of semi-local DFT to describe weak interactions [98, 99]. This well-known problem has resulted in many corrective schemes to account for weak interactions. The semi-classical corrections designed by Grimme are particularly popular, because they can be included at almost no extra cost and give much improved results for weak interactions [97, 100, 101]. A promising alternative are the van der Waals (vdW) density functionals of Langreth–Lundqvist type [102–104], but they depend strongly on the exchange functionals used [105]. From the wavefunction perspective,

highly accurate interaction energies for weakly bound systems can be obtained using CCSD(T), but the steep $O(N^7)$ scaling of this method prohibits application to larger systems. A less costly alternative is MP2, but here long-range interactions are only included at the uncoupled monomer level, leading to mixed results [98]. In contrast, dispersion is naturally included in RPA in a seamless fashion as RPA describes interaction energies at the coupled monomer level [7]. In addition, RPA is the only method apart from CCSD(T) to properly capture the non-pairwise-additive nature of long-range interactions [106, 107].

The random phase approximation was applied extensively to weakly bound dimers, where non-covalent interactions play a crucial role [47, 108]. Here, RPA describes the long-range part of the PES correctly, but underbinds around the equilibrium distance and gives somewhat too large equilibrium bond distances.

Figure 5 shows errors in the relative energies of *n*-butane, *n*-hexane, and *n*-pentane conformers for several methods [86]. Quadruple-zeta basis sets (def2-QZVP, Ref. [85]) were used throughout. The average isomer energy difference is only 1.8 kcal/mol [109]. The branched conformers are more stable than the linear ones, due to the medium-range electronic interactions between bonds. Semi-local DFT fails to include these medium-range interactions and, therefore, leads to incorrect relative energetics for these systems, with errors that are of equal magnitude to the average isomer energy difference. RPA yields a spectacular improvement over semi-local DFT; the errors are now similar to the errors in the reference method. Grimme's double-hybrid B2PLYP [94], which adds a correction based on MP2 theory, is not accurate for this set, but better results are obtained when adding a semi-empirical dispersion correction, particularly the recent -D3 correction [100, 110]. The Minnesota functional M06-2X [111, 112] yields smaller errors than the semi-local functionals, but does not reach the accuracy of RPA. MP2 performs well; somewhat surprisingly, the spin-component-scaled version of MP2 [113] leads to slightly inferior results. Overall, RPA performs very well for these systems where intramolecular medium-range interactions play a crucial role. Its accuracy is comparable to the best available density functionals, such as B2PLYP-D3 and M06-2X, but without any empirical parameters.

The S22 set, designed by Jurecka et al. [115], is a widely used benchmark for weak interactions in biologically relevant systems. The set consists of 22 small- to medium-size dimers, of which 7 systems are primarily hydrogen bound and 8 dispersion bound; the remaining systems contain both interactions. Accurate theoretical reference results are available for this test set [114].

Figure 6 compares RPA results for the S22 set with other commonly used functionals and wave function-based methods. The MAE for RPA is 0.41 kcal/mol, a substantially smaller error than obtained from semi-local DFT,

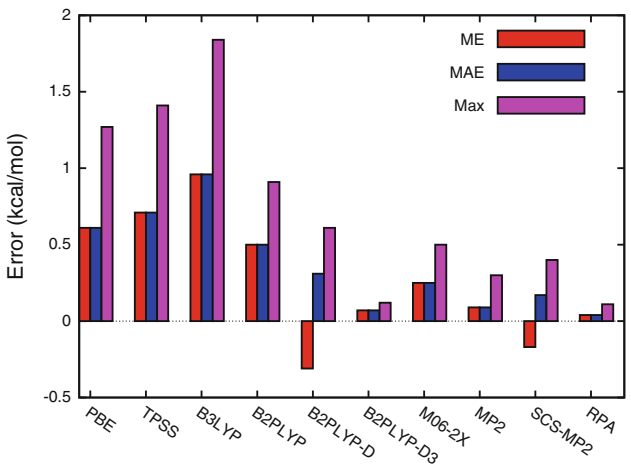

Fig. 5 RPA mean errors (ME), mean absolute errors (MAE), and maximum absolute errors (Max) (kcal/mol) in the relative energies of *n*-alkane conformers compared to other methods. Geometries and reference energies, and non-RPA results were taken from Ref. [110], except for the MP2 and SCS-MP2 results, which were taken from Ref. [109]. def2-QZVP basis sets were used, and no counterpoise correction was applied; the MP2 and SCS-MP2 results were obtained using cc-pVQZ basis sets [82]; RPA results were taken from Ref. [86] and were obtained using self-consistent TPSS orbitals

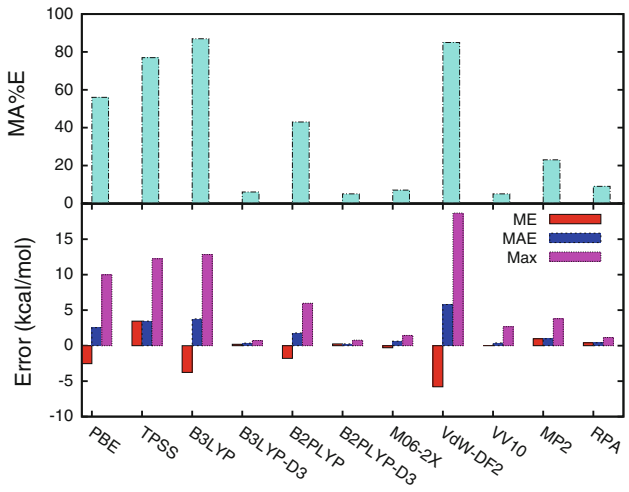

Fig. 6 RPA mean absolute percentage errors (MA%E), mean errors (ME), mean absolute errors (MAE), and maximum absolute errors (Max) (kcal/mol) for the S22 test set compared to other methods. Geometries and reference energies were taken from Ref. [114]. No counterpoise correction was applied, and def2-QZVP basis sets were used, except for the VdW-DF2 and VV10 results [103], which were counterpoise corrected, and were obtained using aug-cc-pVTZ basis sets [82]; RPA results were taken from Ref. [86] and other results from Ref. [110]. RPA results were obtained from self-consistent TPSS orbitals

which seriously fails. The addition of a dispersion correction improves results for semi-local DFT considerably, reducing the MAE to 0.36 kcal/mol for B3LYP-D. The M06-2X functional yields errors of the same order of magnitude [111]. MP2 errors are somewhat larger [110, 115], which is not surprising given the well-known mixed performance of MP2 for dispersion interactions [98]. The recent non-local van der-Waals functional by Vydrov and van Voorhis yields results comparable to RPA, though with a larger maximum error [103]. The vdW-DF2 functional has mean errors comparable to MP2, but with a very large maximum error [103]. In comparison, RPA yields interaction energies of high accuracy (MAE = 0.41 kcal/mol), though it appears that results for weakly bound systems may not be fully converged with respect to basis set size. Further work to assess the basis set convergence of RPA shows an increase of the RPA MAE to 0.82 kcal/mol in the basis set limit. Changing input orbitals from TPSS to self-consistent PBE orbitals hardly effects the errors (MAE = 0.37 kcal/mol). This is in line with previous results [116, 117], showing little variation of the results with the choice of semi-local functional used to compute the orbitals.

Eshuis and Furche [86] applied RPA to the predissociation of a second-generation Grubbs catalyst used for olefin metathesis [118, 119]. The dissociation energy of this complex depends strongly on the medium-range interactions between the bulky ligands [120–122]. Semi-local DFT fails badly with errors of more than half of the experimental dissociation enthalpy of 36.8 kcal/mol [120]. Addition of dispersion corrections reduces the error. Of the Minnesota family of functionals, the M06 and M06-2X functionals achieve high accuracy. RPA improves much upon semi-local DFT, but does not achieve the accuracy of M06-2X. The error in RPA is possibly due to the poor description of short-range correlation within RPA, which is important here because of bond-breaking.

Though results of comparable accuracy can be achieved with other methods, RPA is the only one that is simultaneously parameter-free, non-dependent on a partitioning of the system and computationally efficient. In addition, RPA does not break down for zero-gap systems.

4.2 Self-interaction error and static correlation

Figure 7 shows the PES for H_2 obtained from several methods [53]. Stretched H_2 is a prototype for static correlation; at infinite separation, the orbital energies for the two electrons are exactly degenerate. RPA based on a closed-shell reference determinant describes this limit correctly [53, 123]. On the other hand, the RPA correlation energy in this limit is non-zero, due to the inherent one-electron self-interaction of direct RPA. Semi-local density functionals lead to large errors in the dissociation limit. Spin symmetry breaking produces qualitatively correct potential energy curves, but also causes unphysical spin-polarization. RPA, in contrast, leads to the correct dissociation limit based on a single-determinant *singlet* reference state [123]. RPA (EXX) also leads to the correct limit [140].

SOSEX rigorously removes all one-electron self-interaction, as demonstrated by Henderson and Scuseria [53]. But it simultaneously destroys the correct asymptotic behavior, due to non-vanishing ionic terms in the pair density. Self-interaction error causes RPA to fail completely for (effective) single electron cases such as H_2^+ and He_2^+ (Fig. 8), because of many-electron self-interaction error. Here, SOSEX improves the dissociation limit greatly, by largely eliminating the self-interaction error. In short, SOSEX removes the one-electron self-interaction error, reduces the many-electron self-interaction error, but also removes some desirable left–right correlation.

At medium range, the RPA curve has an unphysical maximum, which is also observed in N_2 [18] and in the challenging case of Be_2 dimer [47]. It has been speculated that the origin of this bump is due to self-interaction error or due to the non-self-consistent nature of the RPA scheme [53]. Though RPA underbinds at the equilibrium distance, it gives good equilibrium bond lengths compared to experiment.

4.3 Atomization energies

The random phase approximation systematically underbinds in molecular atomization energy benchmarks [18].

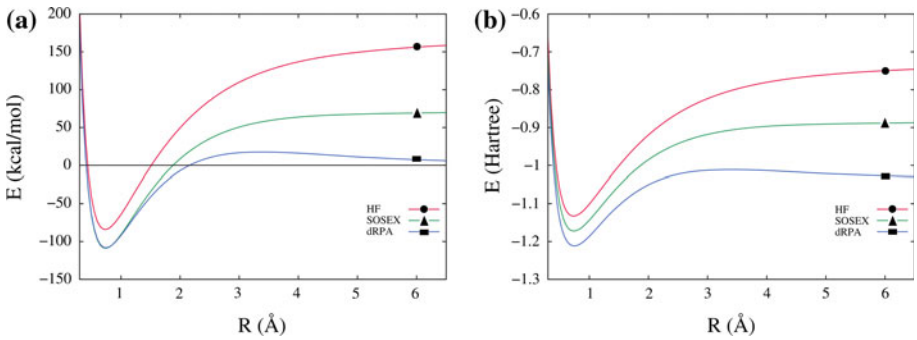

Fig. 7 H_2 dissociation curves for RPA and SOSEX evaluated with self-consistent PBE orbitals using aug-cc-pVQZ basis sets: **a** relative to two H atoms, **b** on an absolute energy scale. (Reprinted with permission from Ref. [53]. Copyright 2010 Taylor & Francis.) The *circle*, *rectangle*, and *triangle* symbols were added to help distinguish the *curves*

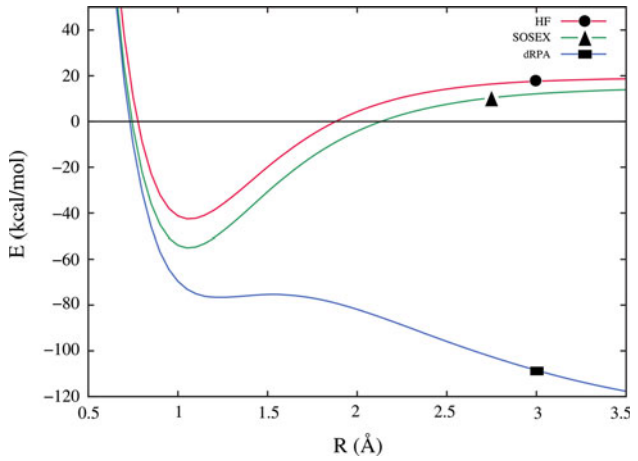

Fig. 8 Dissociation of He_2^+ for RPA and SOSEX evaluated with self-consistent PBE orbitals using aug-cc-pVQZ basis sets. (Reprinted with permission from Ref [53]. Copyright 2010 Taylor & Francis.) The *circle*, *rectangle*, and *triangle* symbols were added to help distinguish the *curves*

Table 1 Calculated atomization energies (kcal/mol) compared to experiment

System	PBE	x-only	RPA	RPA+	Expt.[a]
H_2	105	84	109	110	109
N_2	244	111	223	223	228
O_2	144	25	113	111	121
F_2	53	−43	30	29	38
Ne_2[b]	0.11	−0.15	0.01	−0.08	0.08[c]
Si_2	81	38	70	70	75
HF	142	96	133	132	141
CO	269	170	244	242	259
CO_2	416	234	364	360	389[d]
C_2H_2	415	291	381	378	405[d]
H_2O	234	155	223	222	232[d]
C_6H_5–H[e]	115	100	112	112	120 ± 1[f]

Dunning's cc-pVQZ and cc-pV5Z basis sets [82] were used. Results were obtained using 4–5 extrapolation and basis set superposition correction. (Reprinted with permission from Ref. [18]. Copyright 2001 APS)

[a] Ref. [124], unless otherwise stated

[b] All electron results

[c] Ref. [125]

[d] Ref. [126]

[e] TZVPP basis, no counterpoise

[f] Ref. [127]

Table 1 lists RPA results for small molecules and compares them to other methods [18]. RPA errors are of the same order of magnitude as semi-local DFT. Similar results were obtained by Harl et al. [117] for 24 solids. The relatively poor performance of RPA for atomization energies might be linked to its deficient description of short-range correlation: in the process of atomization, all covalent bonds are broken, leading to large rearrangements of the electronic structure at short-range. RPA+ [43] does not improve upon RPA for atomization energies [18, 34, 117], though it corrects total correlation energies to a large extent.

The good performance for atomization energies of many semi-empirical density functionals is linked to the inclusion of atomization energies in the fitting reference set. The behavior of RPA is similar to non-empirical wavefunction-based methods; as shown for *n*-homodesmotic reactions, RPA errors become systematically smaller with decreasing change in the electronic environment [86, 128], see Sect. 4.5.

Table 2 Mean errors (ME), mean absolute errors (MAE), and maximum errors (Max) (kcal/mol) for the G21IP ionization potential test set for various density functionals using def2-QZVP basis sets

	PBE	TPSS	B3LYP	B2PLYP	RPA[a]
ME	−0.12	−0.87	−0.12	−0.73	−5.01
MAE	3.85	3.95	3.55	2.31	5.11
Max	10.17	11.74	9.59	5.89	13.96

Core electrons were kept frozen; RPA results were obtained from self-consistent TPSS orbitals. Geometries, reference energies, and non-RPA results were taken from Ref. [129]. See supporting information for complete results

[a] Computed for this review

Table 3 Mean errors (ME), mean absolute errors (MAE), and maximum errors (Max) (kcal/mol) for the G21EA electron affinities test set for various density functionals using def2-QZVP basis sets

	PBE	TPSS	B3LYP	B2PLYP	RPA[a]
ME	2.96	0.42	0.30	−0.79	−0.70
MAE	3.43	2.21	1.81	1.37	3.02
Max	7.72	5.83	2.33	3.84	21.60

Core electrons were frozen for the RPA correlation energy calculations. RPA results were obtained from self-consistent TPSS orbitals. Geometries, reference energies, and non-RPA results were taken from Refs. [129] and [110]. See supporting information for complete results

[a] Computed for this review

4.4 Ionization potentials and electron affinities

Jiang and Engel [116] first published RPA ionization potentials for atoms. They found that the semi-local functional BLYP performs better than RPA, but also report a significant improvement for RPA+. Here, we present a more extended set of ionization potentials and electron affinities that include molecular systems. Tables 2 and 3 compare RPA errors in ionization potentials and electron

Table 4 Mean errors (ME), mean absolute errors (MAE), and maximum errors (Max) (kcal/mol) for the BH76RC reaction energy set for various density functionals. def2-QZVP basis sets were used and core electrons were kept frozen

	PBE	TPSS	B3LYP	B2PLYP	RPA/PBE[a]	RPA/TPSS[a]
ME	0.96	0.59	−0.25	−0.11	−0.05	0.39
MAE	4.33	3.78	2.34	1.17	2.61	1.89
Max	22.69	12.90	7.24	5.16	8.75	4.55

RPA results were obtained from self-consistent TPSS or self-consistent PBE orbitals. Geometries, reference energies, and non-RPA results taken from Ref. [129]. See supporting information for complete results

[a] Computed for this review

Table 5 Mean Error (ME), mean absolute error (MAE), and maximum error (Max) (kcal/mol) for the G2RC test set for various density functionals using def2-QZVP basis sets

	PBE	TPSS	B3LYP	B2PLYP	RPA[a]
ME	0.32	3.12	0.53	−0.22	−1.03
MAE	6.20	6.42	2.60	1.71	2.72
Max	18.96	19.97	7.00	5.63	14.47

Core electrons were kept frozen. RPA results were obtained from self-consistent TPSS orbitals. Geometries, reference energies and non-RPA results taken from Ref. [129]. See supporting information for complete results

[a] Computed for this review

Table 6 Mean errors (ME), mean absolute errors (MAE), and maximum errors (Max) (kcal/mol) for the BH76 barrier heights test set for several density functionals using def2-QZVP basis sets

	PBE	TPSS	B3LYP	B2PLYP	RPA/PBE[a]	RPA/TPSS[a]
ME	−9.18	−8.55	−4.56	−2.08	−1.65	−1.79
MAE	9.23	8.57	4.66	2.24	3.10	2.77
Max	−30.68	−23.60	−10.98	−6.47	−11.4	−11.19

Core electrons were kept frozen. RPA results were obtained from either self-consistent TPSS or self-consistent PBE orbitals. Geometries, reference energies, and non-RPA results taken from Ref. [129]. See supporting information for complete results

[a] Computed for this review

affinities for the G21 set to other methods [129]. In contrast to other results presented here, these reactions are not isoelectronic, that is, they do not conserve the number of electrons. The errors for RPA are larger than those of semi-local functionals. However, the nearly equal magnitude of the ME and MAE for the ionization potentials in RPA suggests that RPA lends itself well to systematic improvement. Due caution is necessary for electron affinities, which do not have a well-defined basis set limit if a semi-local density functional is used [130].

4.5 Reaction energies

The accurate calculation and prediction of reaction energies are of great importance for thermochemistry. Most chemical processes involve covalent bondbreaking and making. In recent work, Eshuis and Furche [86] assessed the quality of RPA for the *n*-homodesmotic reaction hierarchy presented by Wheeler et al. [128]. They showed that for isogyric and isodesmic reactions, which involve bondbreaking and making typical for chemical reactions, RPA leads to smaller errors than B3LYP or M06-2X.

Here, we present new results for two test sets. Table 4 contains results for a subset of the 76 reactions studied for barrier heights (*cf.* Sect. 4.6) [129], and Table 5 shows results for a subset of the G2/97 test set. See the supporting information for complete results.

The G2/97 subset consists of 25 reactions involving closed-shell molecules containing first and second row elements [129]. The reaction energies vary from just 1 kcal/mol to over 200 kcal/mol. RPA achieves an accuracy comparable to B3LYP, but with a larger maximum error. The double-hybrid B2PLYP performs somewhat better. The MAE for RPA is approximately two times smaller than the MAE for the PBE or TPSS functional. Similar results are observed for the BH76 subset, which consists of 30 reactions involving atoms and small molecules containing first and second row elements. Here, open-shell free atoms and molecules as well as anions are present, making this a challenging set for semi-local DFT. The reaction energies vary from 1 to 100 kcal/mol. Two sets of RPA results are presented to show that for these energy differences, a relatively large dependence on the input orbitals is observed. It is likely that this is caused by the open-shell atoms and anions, which pose a particular challenge for semi-local DFT. In summary, RPA is accurate even for non-isodesmic reactions, rivaling B3LYP as a general purpose functional for reaction energies.

4.6 Barrier heights

Table 6 shows errors in RPA results compared to other functionals for 76 barrier heights of hydrogen and heavy-atom transfers, nucleophilic substitution, unimolecular and association reactions [129]. The set consists of 38 reactions, and results for forward and backward barriers are presented. The average barrier height is 18.5 kcal/mol, and the reference energies are obtained from W1 and theoretical estimates. GGA functionals fail with MAEs of approximately 40% of the average barrier height. B3LYP improves upon that considerably, while B2PLYP performs best, though chemical accuracy is not reached. RPA performs at the same level as B2PLYP. Grimme's dispersion

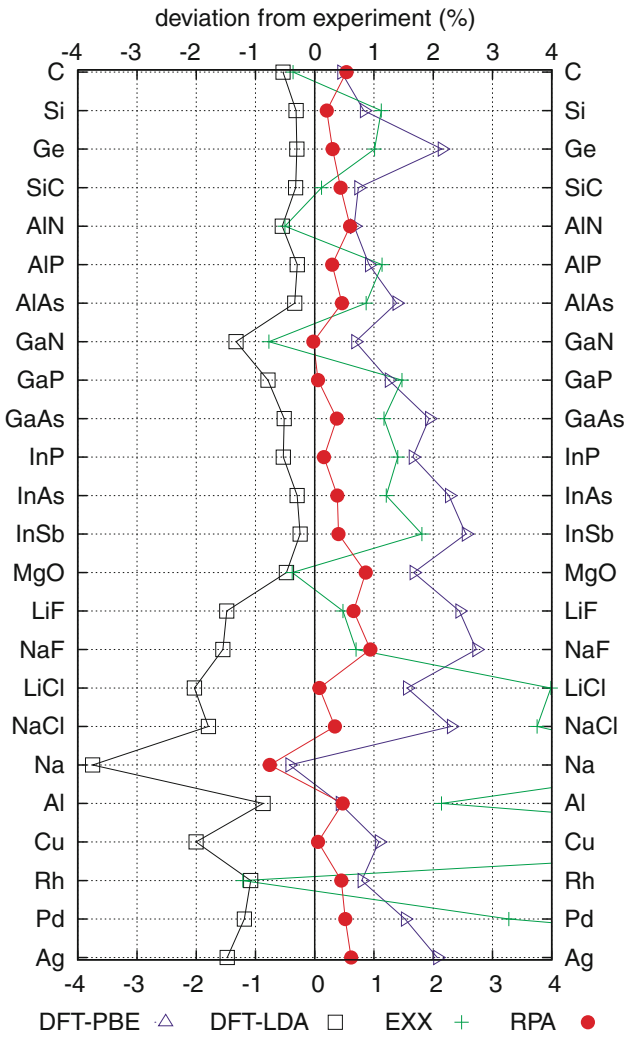

Fig. 9 Relative error (%) of theoretical lattice constants with respect to experiment. (Reprinted with permission from Ref [117]. Copyright 2010 The American Physical Society)

correction does not seem to improve barrier heights. These data show, that RPA is also promising for chemical kinetics.

4.7 Adsorption on surfaces and solid-state properties

Ren et al. [90] applied RPA to the adsorption of CO on a Cu(111) surface. The results were compared to two GGA functionals, PBE and AM05, and two hybrid functionals, PBE0 and HSE03. RPA adsorption energies were found to be most accurate. Importantly, RPA correctly predicts the atop site to be preferred for adsorption over the hollow site. The latter is preferred by the GGA functionals, whereas the hybrid functionals yield a slight preference for the atop site.

Harl et al. [117] evaluated lattice constants for a set of insulators, semiconductors, and metals. RPA using PBE orbitals improves considerably upon semi-local DFT (Fig. 9). In contrast to semi-local DFT, RPA errors do not increase with system size. Similar results were found for bulk moduli and heats of formation. The influence of the input orbitals was found to be small, when starting from LDA orbitals instead of PBE orbitals.

In recent work, Lebègue et al. [131] studied the cohesive properties of graphite using RPA. Graphite is the parent compound of carbon-based materials, which have drawn much interest, both experimentally and theoretically. Of special interest is the interaction between graphene sheets. Here, van der Waals interactions play a crucial role. LSDA binding energies (24 meV/atom) are significantly too small, compared to quantum Monte Carlo results (56 ± 5 meV/atom).

Using RPA, the interlayer equilibrium distance, the elastic constant, and the net layer binding energy were found to be in excellent agreement with experiment, though the computed binding energy of 48 meV/atom is 15% smaller than the binding energy obtained from quantum Monte Carlo methods. In comparison with vdW-type functionals, RPA is more accurate for all three computed properties, though computationally significantly more expensive. It was also found that the correlation energy behaves as $1/d^3$ for large interlayer distances d, in agreement with previous analytical work [132, 133]. This illustrates that RPA captures the non-pairwise additive character of the long-range interactions.

5 Conclusions

RPA has many attractive features: (1) It dramatically improves upon semi-local density functionals for non-covalent interactions; (2) it is non-perturbative and finite for small-gap systems and thus more widely applicable than perturbation theory; (3) it is compatible with 100% exact exchange and captures significant static correlation; (4) it is based on sound physics and does not contain empirical parameters; (5) it is computationally affordable for molecules with well over 100 atoms. For chemical processes that conserve the number of electron pairs, RPA rivals the best available methods in the size range >20 atoms.

Nevertheless, there is room for improvement, especially for processes that change the number of electron pairs. In many ways, RPA is to the correlation energy what the Hartree energy is to the total ground-state energy: An important part that captures essential physics and chemistry, yet is not sufficient for many purposes. But this analogy also suggests that the development of beyond-RPA exchange and correlation methods is a worthwhile endeavor.

Acknowledgments The authors would like to acknowledge Asjbörn Burow for helpful comments. Two of us (H.E. and JE.B.) thank TURBOMOLE GmbH for support. This work was supported by the National Science Foundation, grant No. CHE-0911266.

References

1. Bohm D, Pines D (1951) Phys Rev 82:625
2. Pines D, Bohm D (1952) Phys Rev 85:338
3. Bohm D, Pines D (1953) Phys Rev 92:609
4. Gell-Mann M, Brueckner KA (1957) Phys Rev 106:364
5. McLachlan AD, Ball MA (1964) Rev Mod Phys 36:844
6. Oddershede J (1978) Adv Quant Chem 11:275
7. Szabo A, Ostlund NS (1977) J Chem Phys 67:4351
8. Shibuya T-I, McKoy V (1970) Phys Rev A 2:2208
9. Ostlund N, Karplus M (1971) Chem Phys Lett 11:450
10. Öhrn Y, Linderberg J (1979) Int J Quant Chem 15:343
11. Langreth DC, Perdew JP (1975) Solid State Commun 17:1425
12. Langreth DC, Perdew JP (1977) Phys Rev B 15:2884
13. Gunnarsson O, Lundqvist BI (1976) Phys Rev B 13:4274
14. Callen HB, Welton TA (1951) Phys Rev 83:34
15. Andersson Y, Langreth DC, Lundqvist BI (1996) Phys Rev Lett 76:102
16. Dobson JF, Wang J (1999) Phys Rev Lett 82:2123
17. Dobson J (2006) In: Time-dependent density functional theory, vol. 706. Springer, Berlin, p 443
18. Furche F (2001) Phys Rev B 64:195120
19. Levy M (1979) Proc Natl Acad Sci USA 76:6062
20. Fetter AL, Walecka JD (1971) Quantum theory of many-particle systems, international series in pure and applied physics. MacGraw-Hill, New York
21. Runge E, Gross EKU (1984) Phys Rev Lett 52:997
22. Petersilka M, Gossmann UJ, Gross EKU (1996) Phys Rev Lett 76:1212
23. Casida ME (1995) In: Chong DP (ed) Recent advances in density functional methods, vol. 1 of Recent advances in computational chemistry. World Scientific, Singapore, p 155
24. Furche F (2001) J Chem Phys 114:5982
25. Furche F (2008) J Chem Phys 129:114105
26. Hedin L (1965) Phys Rev 139:A796
27. Toulouse J, Zhu W, Ángyán JG, Savin A (2010) Phys Rev A 82:032502
28. Hellgren M, von Barth U (2007) Phys Rev B 76:075107
29. Onida G, Reining L, Rubio A (2002) Rev Mod Phys 74:601
30. Bechstedt F, Fuchs F, Kresse G (2009) Phys Status Solidi (B) 246:1877
31. Møller C, Plesset MS (1934) Phys Rev 46:618
32. Ball MA, McLachlan AD (1964) Mol Phys 7:501
33. Toulouse J, Gerber IC, Jansen G, Savin A, Ángyán JG (2009) Phys Rev Lett 102:096404
34. Furche T, Van Voorhis T (2005) Chem Phys 122:164106
35. Klopper W, Teale AM, Coriani S, Pedersen TB, Helgaker T (2011) Chem Phys Lett 510:147
36. Jansen G, Liu RF, Ángyán JG (2010) J Chem Phys 133:154106
37. Heßelmann A (2011) J Chem Phys 134:204107
38. Freeman DL (1977) Phys Rev B 15:5512
39. Scuseria GE, Henderson TM, Sorensen DC (2008) J Chem Phys 129:231101
40. Hansen AE, Bouman TD (1979) Mol Phys 37:1713
41. Sanderson EA (1965) Phys Lett 19:141
42. Burke K, Perdew JP, Langreth DC (1994) Phys Rev Lett 73:1283
43. Yan Z, Perdew JP, Kurth S (2000) Phys Rev B 61:16430
44. Ruzsinszky A, Perdew JP, Csonka GI (2010) J Chem Theory Comput 6:127
45. Ruzsinszky A, Perdew JP, Csonka GI (2011) J Chem Phys 134:114110
46. Janesko BG, Henderson TM, Scuseria GE (2009) J Chem Phys 130:081105
47. Zhu W, Toulouse J, Savin A, Ángyán JG (2010) J Chem Phys 132:244108
48. Görling A, Levy M (1993) Phys Rev B 47:13105
49. Ernzerhof M (1996) Chem Phys Lett 263:499
50. Grüneis A, Marsman M, Harl J, Schimka L, Kresse G (2009) J Chem Phys 131:154115
51. Paier J, Janesko BG, Henderson TM, Scuseria GE, Grüneis A, Kresse G (2010) J Chem Phys 132:094103
52. Paier J, Janesko BG, Henderson TM, Scuseria GE, Grüneis A, Kresse G (2010) J Chem Phys 133:179902
53. Henderson TM, Scuseria GE (2010) Mol Phys 108:2511
54. Ren XG, Tkatchenko A, Rinke P, Scheffler M (2011) Phys Rev Lett 106:153003
55. Singwi KS, Tosi MP, Land RH, Sjölander A (1968) Phys Rev 176:589
56. Gross EKU, Kohn W (1990) Adv Quant Chem 21:255
57. Dobson JF, Wang J (2000) Phys Rev B 62:10038
58. Lein M, Gross EKU, Perdew JP (2000) Phys Rev B 61:13431
59. Dobson JF, Wang J, Gould T (2002) Phys Rev B 66:081108
60. Dobson JF (2009) Phys Chem Chem Phys 11:4528
61. Constantin LA, Pitarke JM, Dobson JF, Garcia-Lekue A, Perdew JP (2008) Phys Rev Lett 100:036401
62. Kotani T, Akai H (1998) J Magn Magn Mater 177(181):569
63. Hellgren M, von Barth U (2008) Phys Rev B 78:115107
64. Hirata S, Ivanov S, Grabowski I, Bartlett RJ (2002) J Chem Phys 116:6468
65. Shigeta Y, Hirao K, Hirata S (2006) Phys Rev A 73:010502
66. Heßelmann A, Ipatov A, Görling A (2009) Phys Rev A 80:012507
67. Heßelmann A, Görling A (2010) Mol Phys 108:359
68. Beebe N, Linderberg J (1977) Int J Quant Chem 12:683
69. Friesner RA (1991) Ann Rev Phys Chem 42:341
70. Ko C, Malick DK, Braden DA, Friesner RA, Martínez TJ (2008) J Chem Phys 128:104103
71. Baerends EJ, Ellis DE, Ros P (1973) Chem Phys 2:41
72. Dunlap BI, Connolly JWD, Sabin JRJ (1979) Chem Phys 71:3396
73. Eichkorn K, Treutler O, Öhm H, Häser M, Ahlrichs R (1995) Chem Phys Lett 240:283
74. Bauernschmitt R, Hser M, Treutler O, Ahlrichs R (1997) Chem Phys Lett 264:573
75. Neese F, Olbrich G (2002) Chem Phys Lett 362:170
76. Rappoport D, Furche F (2005) J Chem Phys 122:064105
77. Weigend F, Häser M, Patzelt H, Ahlrichs R (1998) Chem Phys Lett 294:143
78. Weigend F, Häser M (1997) Theor Chim Acta 97:331
79. Eshuis H, Yarkony J, Furche F (2010) J Chem Phys 132:234114
80. Hale N, Higham NJ, Trefethen LN (2008) SIAM J Num Anal 46:2505
81. Boyd JP (1987) J Sci Comput 2:99
82. Dunning J (1989) J Chem Phys 90:1007
83. Weigend F, Köhn A, Hättig C (2002) J Chem Phys 116:3175
84. Tajti A, Szalay PG, Császár AG, Kállay M, Gauss J, Valeev EF, Flowers BA, Vázquez J, Stanton JF (2004) J Chem Phys 121:11599
85. Weigend F, Ahlrichs R (2005) Phys Chem Chem Phys 7:3297
86. Eshuis H, Furche F (2011) J Phys Chem Lett 2:983
87. Harl J, Kresse G (2008) Phys Rev B 77:045136
88. Fuchs M, Gonze X (2002) Phys Rev B 65:235109
89. Niquet YM, Fuchs M, Gonze X (2003) Phys Rev A 68:032507

90. Ren X, Rinke P, Scheffler M (2009) Phys Rev B 80:045402
91. Bashford D, Chothia C, Lesk AM (1987) J Mol Biol 196:199
92. Dabkowska I, Gonzalez HV, Jurecka P, Hobza P (2005) J Phys Chem A 109:1131
93. Meyer EA, Castellano RK, Diederich F (2003) Angew Chem Int Ed 42:1210
94. Grimme S (2006) J Chem Phys 124:034108
95. Kemnitz CR, Mackey JL, Loewen MJ, Hargrove JL, Lewis JL, Hawkins WE, Nielsen AF (2010) Chem Eur J 16:6942
96. Wodrich MD, Jana DF, von Rague Schleyer P, Corminboeuf C (2008) J Phys Chem A 112:11495
97. Grimme S, Djukic J (2010) Inorg Chem 49:2911
98. Sherrill CD (2009) In: Rev Comp Chem, Wiley, New York, pp 1–38
99. Černý J, Hobza P (2007) Phys Chem Chem Phys 9:5291
100. Schwabe T, Grimme S (2007) Phys Chem Chem Phys 9:3397
101. Grimme S (2004) J Comp Chem 25:1463
102. Dion M, Rydberg H, Schröder E, Langreth DC, Lundqvist BI (2004) Phys Rev Lett 92:246401
103. Vydrov OA, Van Voorhis T (2010) Phys Rev A 81:062708
104. Vydrov OA, Van Voorhis T (2009) J Chem Phys 130:104105
105. Langreth D, Lundqvist B, Chakarova-Käck S, Cooper V, Dion M, Hyldgaard P, Kelkkanen A, Kleis J, Kong L, Li S et al (2009) J Phys Cond Matter 21:084203
106. Axilrod BM, Teller E (1943) J Chem Phys 11:299
107. Lu D, Nguyen H, Galli G (2010) J Chem Phys 133:154110
108. Janesko BG, Scuseria GE (2009) J Chem Phys 131:154106
109. Gruzman D, Karton A, Martin JML (2009) J Phys Chem A 113:11974
110. Goerigk L, Grimme S (2011) Phys Chem Chem Phys 13:6670
111. Zhao Y, Truhlar DG (2008) Acc Chem Res 41:157167
112. Zhao Y, Truhlar DG (2011) Chem Phys Lett 502:1
113. Grimme S (2005) J Phys Chem A 109:3067
114. Takatani T, Hohenstein EG, Malagoli M, Marshall MS, Sherrill CD (2010) J Chem Phys 132:144104
115. Jurecka P, Sponer J, Cerny J, Hobza P (2006) Phys Chem Chem Phys 8:1985
116. Jiang H, Engel E (2007) J Chem Phys 127:184108
117. Harl J, Schimka L, Kresse G (2010) Phys Rev B 81:115126
118. Vougioukalakis GC, Grubbs RH (2010) Chem Rev 110:1746
119. Sanford MS, Love JA, Grubbs RH (2001) J Am Chem Soc 123:6543
120. Śliwa P, Handzlik J (2010) Chem Phys Lett 493:273
121. Zhao Y, Truhlar DG (2009) J Chem Theory Comput 5:324
122. Benitez D, Tkatchouk E, Goddard WA (2009) Organometallics 28:2643
123. Fuchs M, Niquet Y-M, Gonze X, Burke K (2005) J Chem Phys 122:094116
124. Huber KP, Herzberg G (1979) Constants of diatomic molecules, vol. IV of Molecular spectra and molecular structure. Van Nostrand Reinhold, New York
125. Oglivie JF, Wang FYH (1992) J Mol Struct 273:277
126. Adamo C, Ernzerhof M, Scuseria GE (2000) J Chem Phys 112:2643
127. May K, Dapprich S, Furche F, Unterreiner BV, Ahlrichs R (2000) Phys Chem Chem Phys 2:5084
128. Wheeler SE, Houk KN, vR Schleyer P, Allen WD (2009) J Am Chem Soc 131:2547
129. Goerigk L, Grimme S (2010) J Chem Theory Comput 6:107
130. Lee D, Furche F, Burke K (2010) J Phys Chem Lett 1:2124
131. Lebègue S, Harl J, Gould T, Ángyán JG, Kresse G, Dobson JF (2010) Phys Rev Lett 105:196401
132. Dobson JF, White A, Rubio A (2006) Phys Rev Lett 96:073201
133. Gould T, Simpkins K, Dobson JF (2008) Phys Rev B 77:165134
134. Heßelmann A, Görling A (2011) Mol Phys 109:2473
135. Ángyán JG, Liu R-F, Toulouse J, Jansen G (2011) J Chem Theory Comput 7:3116
136. Toulouse J, Zhu W, Savin A, Jansen G, Ángyán JG (2011) J Chem Phys 135:084119
137. Toulouse J, Zhu W, Ángyán JG, Savin A (2010) Phys Rev A82:032502
138. Irelan RM, Henderson TM, Scuseria GE (2011) J Chem Phys 135:094105
139. Lotrich V, Bartlett RJ (2011) J Chem Phys 134:184108
140. Heßelmann A, Görling A (2011) Phys Rev Lett 106:093001